

Simulating Majorana zero modes on a noisy quantum processor

Kevin J. Sung,^{1,*} Marko J. Rančić,² Olivia T. Lanes,¹ and Nicholas T. Bronn¹

¹*IBM Quantum, IBM T.J. Watson Research Center, Yorktown Heights, NY 10598, USA*

²*TotalEnergies, Tour Coupole La Défense, 2 Pl. Jean Millier, 92078 Paris, France*

(Dated: January 25, 2023)

The simulation of systems of interacting fermions is one of the most anticipated applications of quantum computers. The most interesting simulations will require a fault-tolerant quantum computer, and building such a device remains a long-term goal. However, the capabilities of existing noisy quantum processors have steadily improved, sparking an interest in running simulations that, while not necessarily classically intractable, may serve as device benchmarks and help elucidate the challenges to achieving practical applications on near-term devices. Systems of *non*-interacting fermions are ideally suited to serve these purposes. While they display rich physics and generate highly entangled states when simulated on a quantum processor, their classical tractability enables experimental results to be verified even at large system sizes that would typically defy classical simulation. In this work, we use a noisy superconducting quantum processor to prepare Majorana zero modes as eigenstates of the Kitaev chain Hamiltonian, a model of non-interacting fermions. Our work builds on previous experiments with non-interacting fermionic systems. Previous work demonstrated error mitigation techniques applicable to the special case of Slater determinants. Here, we show how to extend these techniques to the case of general fermionic Gaussian states, and demonstrate them by preparing Majorana zero modes on systems of up to 7 qubits.

I. INTRODUCTION

The simulation of systems of interacting fermions is one of the most anticipated applications of quantum computers due to its value to commercial industry and scientific research [1, 2]. The most interesting simulations will undoubtedly require a fault-tolerant quantum computer capable of executing arbitrarily long quantum programs. The effort to build such a device is underway at academic and industrial institutions, and while fault-tolerance remains a long-term goal, the capabilities of existing prototypes have steadily improved [3–7]. These improved capabilities have sparked an interest in running simulations that, while not necessarily classically intractable, may serve as device benchmarks and help elucidate the challenges to achieving practical applications on near-term devices [8–12].

Systems of *non*-interacting fermions are ideally suited to serve these purposes. Despite being classically tractable, they display rich physics and produce highly entangled states when simulated on a quantum processor. Because they are classically tractable, experimental results can be verified even at large system sizes that would typically defy classical simulation. Previous experimental demonstrations of such simulations include an implementation of the Hartree-Fock method on a quantum processor [12] and the preparation of Majorana zero modes [13]. In both of these experiments, the quantum states prepared and measured belong to the class of fermionic Gaussian states, of which Slater determinants are a special case. Fermionic Gaussian states refer to eigenstates of a quadratic Hamiltonian, the defining feature of a system of non-interacting fermions.

Reference [12] demonstrated that for Slater determinants, the error mitigation techniques of physically-motivated postselection of bitstrings and state purification can be used to significantly improve the fidelity of the simulation and the accuracy of measured observables. In this work, we show that these techniques can be extended to the case of general fermionic Gaussian states, and demonstrate them by improving on the preparation of Majorana zero modes performed in Reference [13]. We also apply some additional error mitigation techniques which were not used in either reference. While Reference [13] ran experiments on only 3 qubits, here our error mitigation techniques enable us to go up to 7 qubits while also obtaining more accurate results. Our experiments are performed on a superconducting qubit processor manufactured at IBM.

Majorana zero modes (MZMs) refer to zero-energy Majorana fermion modes that exhibit topological properties due to spatial separation of the modes. A prototypical system that contains MZMs is the Kitaev chain. The Hamiltonian of a Kitaev chain is

$$\begin{aligned} H = & -t \sum_{j=1}^n \left(a_j^\dagger a_{j+1} + a_{j+1}^\dagger a_j \right) \\ & + \sum_{j=1}^n \left(\Delta a_j^\dagger a_{j+1}^\dagger + \Delta^* a_{j+1} a_j \right) \\ & + \mu \sum_{j=1}^n \left(a_j^\dagger a_j - \frac{1}{2} \right), \end{aligned} \quad (1)$$

where t is the tunneling amplitude, Δ is the superconducting pairing, μ is the chemical potential, and the $\{a_j\}$ are fermionic annihilation operators for a system of n fermionic modes. When $|\Delta| = t > 0$ and $\mu = 0$, the

* email: kevinsung@ibm.com

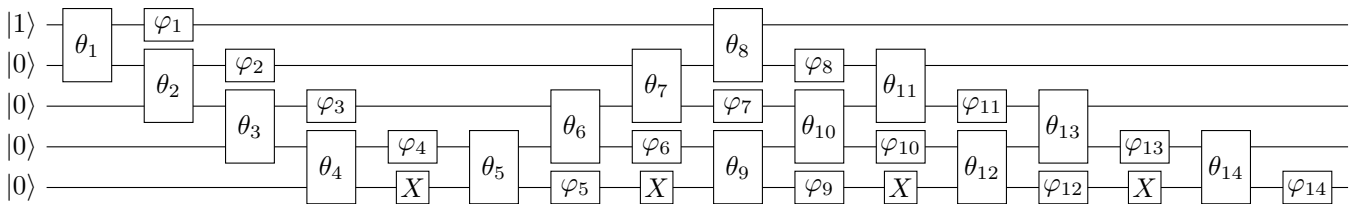


FIG. 1. Circuit to prepare the first excited state of a 5-mode Kitaev chain. Gates labeled with an angle θ are real-valued Givens rotation gates and gates labeled with an angle φ are Z rotations. Note that the presence of the X gates implies that in general, the circuit does not conserve particle number. However, the circuit always prepares a state with a well-defined parity. The Givens rotation gate can be implemented on IBM hardware by decomposing it into 2 CNOT gates plus single-qubit rotations.

Hamiltonian (1) takes the form

$$H = it \sum_{j=2}^{2n-2} \gamma_j \gamma_{j+1} \quad (2)$$

where we have introduced the Majorana fermion operators

$$\gamma_{2j-1} = a_j + a_j^\dagger, \quad \gamma_{2j} = -i(a_j - a_j^\dagger). \quad (3)$$

Note that γ_1 and γ_{2n} do not appear in the Hamiltonian (2); these are unpaired zero-energy Majorana modes localized at the ends of the chain. The energy and separation of the modes is robust to small perturbations in μ . MZMs can theoretically be used as carriers of quantum information with a Clifford gate set which is topologically protected against errors; this fact has motivated efforts at their experimental realization [14].

In this work, we map the Kitaev chain model to a system of qubits using the Jordan-Wigner transformation (JWT). Despite the nonlocal nature of the JWT, eigenstates of the model can be prepared efficiently using only gates acting on neighboring qubits on a line. We measure the excitation energies of the model by separately preparing the ground and excited states, and we observe the presence of zero-energy excitations that are robust to perturbations in μ . We also measure the Majorana site correlation $i\gamma_1\gamma_j$ and observe an exclusive correlation between the ends of the wire at $\mu = 0$ which breaks down with increasing μ .

II. RESULTS

A. Circuits and observable measurement

Since the Kitaev chain Hamiltonian is quadratic in the fermionic creation and annihilation operators, its

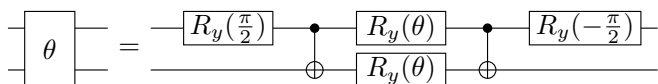


FIG. 2. Decomposition of the Givens rotation gate into two CNOT gates plus single-qubit rotations.

eigenstates are fermionic Gaussian states which can be prepared efficiently using the algorithm given in Reference [15]. This algorithm has linear circuit depth and requires only linear qubit connectivity. It assumes the Jordan-Wigner transform is used to map fermionic operators to qubit operators. Figure 1 displays an example circuit that shows the general structure. Besides single-qubit Z rotations and X gates, the only other type of gate present is the so-called Givens rotation gate, with matrix

$$G(\theta) = \begin{pmatrix} 1 & 0 & 0 & 0 \\ 0 & \cos(\theta) & -\sin(\theta) & 0 \\ 0 & \sin(\theta) & \cos(\theta) & 0 \\ 0 & 0 & 0 & 1 \end{pmatrix}. \quad (4)$$

On hardware for which CNOT is the native two-qubit interaction, this gate can be implemented using the decomposition shown in Figure 2, which uses two CNOT gates in addition to single-qubit rotations.

Eigenstates of a quadratic Hamiltonian are prepared by effecting a basis change that maps the fermionic creation operators $\{a_j^\dagger\}$ to a new set of creation operators $\{b_j^\dagger\}$ such that the Hamiltonian takes the diagonal form

$$H = \sum_j \varepsilon_j b_j^\dagger b_j + \text{constant} \quad (5)$$

where $0 \leq \varepsilon_1 \leq \dots \leq \varepsilon_n$. The operators $\{b_j^\dagger\}$ also satisfy the fermionic anticommutation relations, so they can be regarded as creation operators for fermionic excitations with excitation energies given by $\{\varepsilon_j\}$. The $\{b_j^\dagger\}$ are linear combinations of the original creation and annihilation operators:

$$\begin{pmatrix} b_1^\dagger \\ \vdots \\ b_n^\dagger \end{pmatrix} = W \begin{pmatrix} a_1^\dagger \\ \vdots \\ a_n^\dagger \\ a_1 \\ \vdots \\ a_n \end{pmatrix} \quad (6)$$

where W is an $n \times 2n$ matrix. The matrix W can be efficiently computed from the description of the Hamiltonian and is used to produce the quantum circuit that prepares

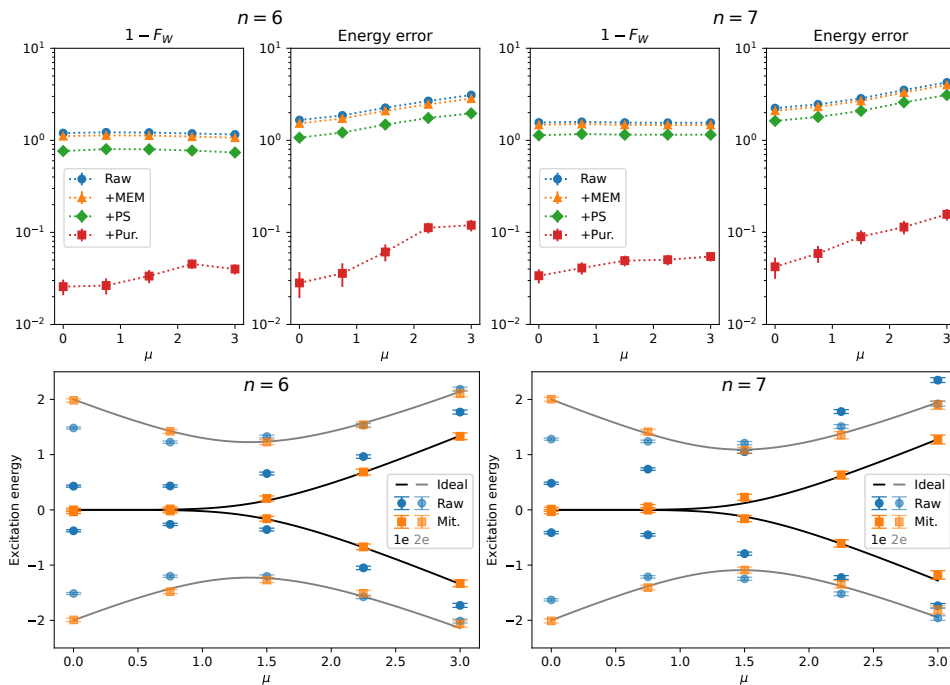


FIG. 3. Fidelity, error, and energy. (Top) One minus the fidelity witness and the average error in energy (expectation value of the Hamiltonian). Note that the fidelity witness is only guaranteed to be a lower bound on the true fidelity, so it can be negative. The data for the 6-mode Kitaev chain is shown on the left, and the data for the 7-mode Kitaev chain is shown on the right. The different lines in each figure correspond to successive applications of error mitigation techniques. As error mitigation is applied, the fidelity witness improves and error decreases. “+MEM” refers to measurement error mitigation. “+PS” refers to postselection of bitstrings based on parity. “+Pur.” refers to purification of the measured correlation matrix. All circuits were executed with dynamical decoupling pulses added. (Bottom) The measured excitation energies of the first and second excitations above the ground state, and their symmetric hole counterparts. “Raw” refers to raw data from circuits executed with dynamical decoupling pulses, and “Mit.” refers to the data after all error mitigation techniques are applied. The signature of Majorana zero modes is the zero-energy first excitation separated from the finite-energy second excitation at $\mu = 0$ and the robustness of this property to perturbations in μ . This property can be clearly seen in the two leftmost data points in each plot. All error bars indicate a confidence interval of two standard deviations (95% confidence) as estimated from the sample covariance.

an eigenstate of the Hamiltonian. In Appendix A, we review the quantum algorithm for preparing fermionic Gaussian states.

For each state prepared, all observables of interest can be determined from the correlation matrix. The correlation matrix Γ of a state ρ is defined as the block matrix

$$\Gamma = \begin{pmatrix} T & S \\ -S^* & I - T^T \end{pmatrix} \quad (7)$$

where

$$T_{jk} = \text{Tr} \left[a_j^\dagger a_k \rho \right] \quad (8)$$

$$S_{jk} = \text{Tr} \left[a_j^\dagger a_k^\dagger \rho \right] \quad (9)$$

and I is the identity matrix.

We measured the correlation matrix using a protocol similar to the one used in Reference [12] to measure the one-particle reduced density matrix (1-RDM), which is the matrix T in our notation.

The diagonal entries of the correlation matrix are occupation numbers that can be measured straightforwardly

in the computational basis. To obtain the off-diagonal entries, we need to measure the operators

$$a_j^\dagger a_k + a_k^\dagger a_j \quad (10)$$

$$-i(a_j^\dagger a_k - a_k^\dagger a_j) \quad (11)$$

$$a_j^\dagger a_k^\dagger + a_k a_j \quad (12)$$

$$-i(a_j^\dagger a_k^\dagger - a_k a_j) \quad (13)$$

Under the Jordan-Wigner transformation, the operators between neighboring modes (i.e., $k = j + 1$) can be measured using a two-qubit basis change. To measure the operators between all pairs of modes, we generate new circuits by permuting the columns of W ; each permutation corresponds to a relabeling of the fermionic modes which cause new pairs to become adjacent. This strategy allows us to measure the operators between all pairs of modes using the same circuit structure. In total, $\lceil n/2 \rceil \times 8 + 1$ different circuits are required to measure the full correlation matrix. In Appendix B, we provide a detailed description of our measurement protocol.

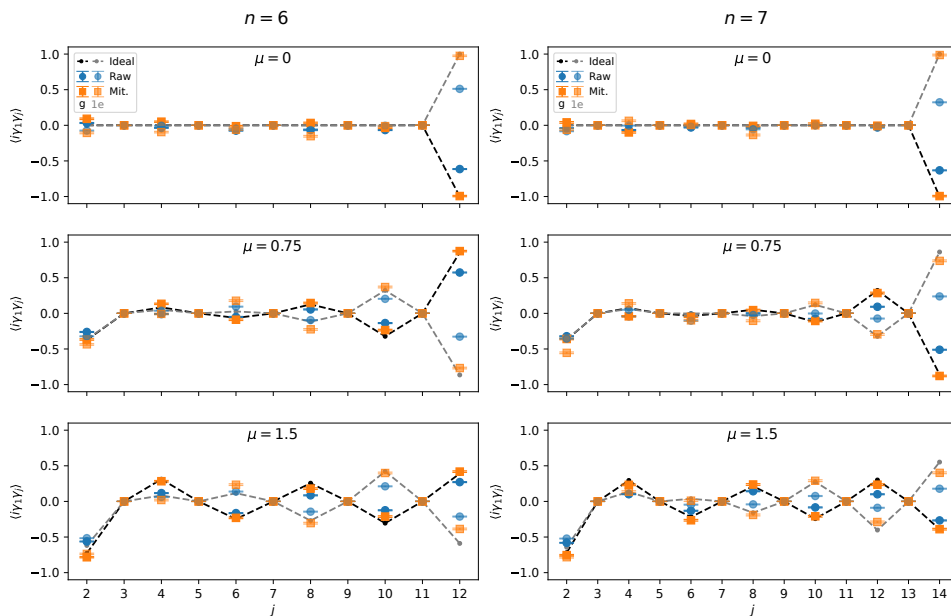


FIG. 4. Majorana site correlation. The Majorana site correlation at site j is defined as the operator $i\gamma_1\gamma_j$ where γ_j denotes the j -th Majorana operator. The data for the 6-mode Kitaev chain is shown on the left, and the data for the 7-mode Kitaev chain is shown on the right. For each system size, we include plots for several different values of μ , as indicated on the plots. Each plot includes data for the ground state (ideal values indicated by the dashed black line) and the first excited state (ideal values indicated by the dashed gray line). “Raw” refers to raw data without error mitigation, and “Mit.” refers to the data after all error mitigation techniques are applied. At $\mu = 0$ the correlation is only nonzero for $j = 2n$, indicating an exclusive correlation between Majorana fermions at the ends of the chain. As μ increases this exclusive correlation breaks down. All error bars indicate a confidence interval of two standard deviations (95% confidence) as estimated from the sample covariance.

B. Error mitigation

We applied a number of error mitigation techniques to improve results.

Dynamical decoupling. Dynamical decoupling is a technique to reduce phase errors stemming from time-correlated low-frequency noise by applying refocusing pulses on idle qubits [16, 17]. There are many possible pulse sequences that could be applied. We used the 4-pulse sequence

$$X_\pi \rightarrow Y_\pi \rightarrow X_{-\pi} \rightarrow Y_{-\pi} \quad (14)$$

where X_π and $X_{-\pi}$ denote X gates implemented using opposite sign pulse amplitudes. We used Qiskit [18] to schedule the dynamical decoupling pulses. The software detects idle periods in the compiled circuit and in each idle period inserts one pulse sequence, distributing the 4 pulses with even temporal spacing.

Measurement error mitigation. The effect of measurement errors can be mitigated by treating it as a classical noise channel and approximately inverting it [19]. We used the software package `mthree` [20, 21] to perform measurement error mitigation. The error mitigation procedure converts raw bitstring counts into error-mitigated bitstring quasiprobabilities. The error mitigation does not come for free; rather, there is increased uncertainty in computed quantities.

Postselection of bitstrings. In Reference [12] which prepared the Hartree-Fock state, the ideal final state had a well-defined particle number, so measured bitstrings with the incorrect particle number could be discarded to improve results. In our case, the final state does not have a well-defined particle number, but it does have a well-defined parity. Therefore, we can still perform postselection on the bitstrings, discarding those with the incorrect parity. A technical detail is that here we actually apply postselection not on the bitstrings directly, but on the quasiprobability distribution over bitstrings returned by the measurement error mitigation procedure. In Table I, we show the quasiprobability mass discarded by the postselection.

State purification. Reference [12] exploited the fact that the 1-RDM is idempotent (it is equal to its square) to perform purification of the measured 1-RDM. That is, due to experimental error, the measured 1-RDM is not idempotent, and it was projected onto the space of idempotent matrices using a procedure called McWeeny purification [22]. In our case, it is the correlation matrix that is idempotent [23]. Therefore, McWeeny purification can also be applied here to purify the measured correlation matrix. The purification is accomplished by repeating until convergence the following numerical operation to update Γ at iteration k :

$$\Gamma_{k+1} = \Gamma_k^2(3I - 2\Gamma_k). \quad (15)$$

System size	Vacuum	Occupied
6 qubits	0.283	0.348
7 qubits	0.344	0.398

TABLE I. Quasiprobability mass discarded by postselection on bitstring parity. The “Vacuum” column indicates circuits where the initial state is the all zeros state; due to an optimization, these circuits had fewer gates than circuits with an “occupied” initial state, and hence a lower expected fraction of bitstrings with the incorrect parity.

C. Experiments

For our experiments, we set $t = -1$, $\Delta = 1$, and used 5 different values for μ evenly spaced between 0 and 3. For each choice of Hamiltonian parameters, we prepared 6 eigenstates: the ground state and the first and second excited states, as well as the 3 corresponding eigenstates from the opposite end of the spectrum. We executed our circuits on the *ibmq_guadalupe* device accessed through the IBM Quantum service. We used Qiskit [18] to compile the circuits into basis gates supported by the hardware. The Givens rotation gates were compiled using a decomposition similar to the one shown in Figure 2, requiring 2 CNOT gates for each Givens rotation. For each circuit we collected 100,000 measurement shots.

To execute each circuit, we needed to pick a line of qubits to use. Because gate errors vary over the device, the choice of qubits can have a significant impact on performance. To pick the qubits, we used the software package *mapomatic* [24], which attempts to minimize the expected error in executing the circuit using a subgraph isomorphism algorithm scored on gate errors reported for the device.

Reference [25] shows how to compute a fidelity witness for experiments that prepare fermionic Gaussian states. The fidelity witness gives a lower bound on the fidelity of the experimentally measured state with the ideal state and can be easily computed from the correlation matrix; see Appendix C for a review of this result. Figure 3 (top panel) shows the fidelity witness and average error in energy.

Figure 3 (bottom panel) shows the measured excitation energies of the first and second excitations above the ground state, and their symmetric hole counterparts. We show both the values obtained from the raw data and those obtained after applying error mitigation.

Figure 4 shows the measured expectation value of the Majorana site correlation $i\gamma_1\gamma_j$. Again, both raw and error-mitigated data are displayed.

III. DISCUSSION

We created Majorana zero modes on a noisy superconducting qubit processor by preparing eigenstates of the Kitaev chain Hamiltonian. The largest chain that we

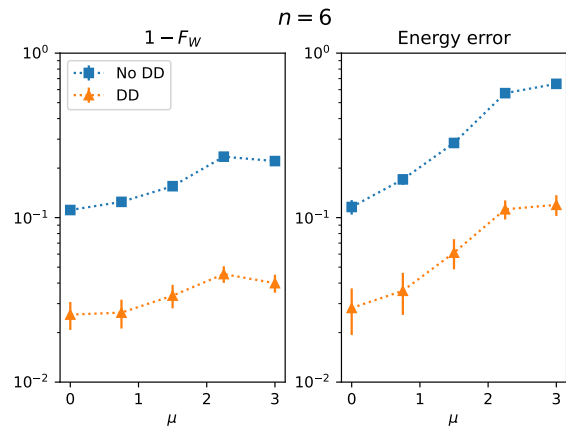


FIG. 5. Effectiveness of dynamical decoupling. This figure shows the fidelity witness and the energy error for experiments without dynamical decoupling (No DD) and with dynamical decoupling (DD) on the Kitaev chain of length 6.

simulated used 7 qubits. Simulating this chain required executing circuits containing dozens of two-qubit gates, yet our experimental results closely matched theory despite their implementation on noisy hardware. We measured zero-energy excitations at $\mu = 0$ which were robust to small perturbations in μ . We also observed the exclusive correlation between Majorana fermions at the ends of the chain at $\mu = 0$ and increasing correlations with interior sites with increasing μ . In the limit of infinite chain length, the value of $\mu = 2t$ separates two topological phases, but with a finite length chain this value is smaller; at $\mu = 1.5t$ in our experiments the correlation between the first site and interior sites is as strong as that between the ends of the chain. At small chemical potential, the wavefunction for a finite-length chain decays exponentially as $\exp(-(j-1)/\xi)$, where j is the site and ξ is the characteristic MZM decay length [26]

$$\xi = 2 \begin{cases} \left| \ln \left(\frac{t-\Delta}{t+\Delta} \right) \right|^{-1} & |t| \geq |\Delta|, \\ \left| \ln \left(\frac{\Delta-t}{\Delta+t} \right) \right|^{-1} & |\Delta| \geq |t|. \end{cases} \quad (16)$$

The quality of our results was made possible by our utilization of error mitigation techniques. We applied dynamical decoupling pulses to idle qubits to mitigate dephasing errors. To see whether these pulses actually improved results, we ran experiments with and without dynamical decoupling (while still applying the rest of the error mitigation techniques). Figure 5 shows the fidelity witness and energy error for these experiments on the 6-mode Kitaev chain. Applying dynamical decoupling pulses does indeed yield a significant improvement, which suggests that low frequency noise on idle qubits is a major source of dephasing error. We also applied measurement error mitigation; this is a straightforward and widely applicable technique that is becoming common practice.

The other techniques we applied were physically-motivated postselection of measured bitstrings and state purification. These techniques have previously been used in the preparation of Slater determinants [12]. Here, we showed how to extend these techniques to the general case of fermionic Gaussian states so they can be used for the preparation of arbitrary eigenstates of quadratic Hamiltonians such as the Kitaev chain Hamiltonian. These techniques were highly effective at improving the fidelity and lowering the error of our simulations.

The combined application of all of these error mitigation techniques enabled us to simulate systems of up to 7 qubits, whereas a previous experiment preparing Majorana zero modes used only 3 qubits. We note that References [27, 28] performed larger experiments (up to 21 and 47 qubits, respectively) with Majorana modes on noisy quantum processors by periodically driving the qubits with a Floquet unitary, implementing time-varying Hamiltonians in both non-interacting and interacting regimes. Those works do not directly prepare eigenstates, but rather extract experimental signatures of the Majorana modes via spectroscopic measurements. This contrasts with our work, which focuses on the exact preparation and measurement of eigenstates of the static Kitaev model.

Although in this work we deal with the non-interacting Kitaev chain model, a modified version of the model with an added interaction term has received much attention [29–34]. The interacting model does not have an analytic solution in the general case. Its eigenstates are not fermionic Gaussian states, so the algorithm we used in this work cannot be applied directly to its solution. However, our work does open the path to the study of the interacting Kitaev chain on quantum computers. Depending on the strength of the interaction, the ground

state of the model may have a non-negligible overlap with the ground state of a non-interacting model. Thus, the ground state of the non-interacting model, prepared using the methods in this work, may be used as the initial state for a variational [35, 36] or adiabatic [37, 38] algorithm for preparing the ground state of the interacting model.

Our results build on previous experiments suggesting that error mitigation will be crucial to achieving practical applications on noisy near-term quantum computers, and they contribute to the growing library of experiments that can serve as device benchmarks as we work towards those practical applications.

Acknowledgments

The authors acknowledge the use of IBM Quantum Services for this work. This experiment was implemented and executed using Qiskit [18]. The circuit diagrams in this paper were created using `qpic` [39]. The data plots were created using Matplotlib [40].

Data availability

The experimental data for this work is available at <https://doi.org/10.5281/zenodo.6603265>.

Code availability

A snapshot of the source code is included at <https://doi.org/10.5281/zenodo.6603265>. An up-to-date version is maintained at <https://github.com/qiskit-research/qiskit-research>.

-
- [1] A. Aspuru-Guzik, A. D. Dutoi, P. J. Love, and M. Head-Gordon, Simulated quantum computation of molecular energies, *Science* **309**, 1704 (2005).
 - [2] I. M. Georgescu, S. Ashhab, and F. Nori, Quantum simulation, *Rev. Mod. Phys.* **86**, 153 (2014).
 - [3] J. Preskill, Quantum Computing in the NISQ era and beyond, *Quantum* **2**, 79 (2018).
 - [4] F. Arute, K. Arya, R. Babbush, D. Bacon, J. C. Bardin, R. Barends, R. Biswas, S. Boixo, F. G. S. L. Brandao, D. A. Buell, B. Burkett, Y. Chen, Z. Chen, B. Chiaro, R. Collins, W. Courtney, A. Dunsworth, E. Farhi, B. Foxen, A. Fowler, C. Gidney, M. Giustina, R. Graff, K. Guerin, S. Habegger, M. P. Harrigan, M. J. Hartmann, A. Ho, M. Hoffmann, T. Huang, T. S. Humble, S. V. Isakov, E. Jeffrey, Z. Jiang, D. Kafri, K. Kechedzhi, J. Kelly, P. V. Klimov, S. Knysh, A. Korotkov, F. Kostritsa, D. Landhuis, M. Lindmark, E. Lucero, D. Lyakh, S. Mandrà, J. R. McClean, M. McEwen, A. Megrant, X. Mi, K. Michielsen, M. Mohseni, J. Mutus, O. Naaman, M. Neeley, C. Neill, M. Y. Niu, E. Ostby, A. Petukhov, J. C. Platt, C. Quintana, E. G. Rieffel, P. Roushan, N. C. Rubin, D. Sank, K. J. Satzinger, V. Smelyanskiy, K. J. Sung, M. D. Trevithick, A. Vainsencher, B. Villalonga, T. White, Z. J. Yao, P. Yeh, A. Zalcman, H. Neven, and J. M. Martinis, Quantum supremacy using a programmable superconducting processor, *Nature* **574**, 505 (2019).
 - [5] K. Wright, K. M. Beck, S. Debnath, J. M. Amini, Y. Nam, N. Grzesiak, J.-S. Chen, N. C. Pistenti, M. Chmielewski, C. Collins, K. M. Hudek, J. Mizrahi, J. D. Wong-Campos, S. Allen, J. Apisdorf, P. Solomon, M. Williams, A. M. DuCore, A. Blinov, S. M. Kreike-meier, V. Chaplin, M. Keesan, C. Monroe, and J. Kim, Benchmarking an 11-qubit quantum computer, *Nature Communications* **10**, 5464 (2019).
 - [6] P. Jurcevic, A. Javadi-Abhari, L. S. Bishop, I. Lauer, D. F. Bogorin, M. Brink, L. Capelluto, O. Günlük, T. Itoko, N. Kanazawa, A. Kandala, G. A. Keefe, K. Kruslich, W. Landers, E. P. Lewandowski, D. T. McClure, G. Nannicini, A. Narasgond, H. M. Nayfeh, E. Pritchett, M. B. Rothwell, S. Srinivasan, N. Sundaresan, C. Wang, K. X. Wei, C. J. Wood, J.-B. Yau, E. J. Zhang, O. E.

- Dial, J. M. Chow, and J. M. Gambetta, Demonstration of quantum volume 64 on a superconducting quantum computing system, *Quantum Science and Technology* **6**, 025020 (2021).
- [7] J. M. Pino, J. M. Dreiling, C. Figgatt, J. P. Gaebler, S. A. Moses, M. S. Allman, C. H. Baldwin, M. Foss-Feig, D. Hayes, K. Mayer, C. Ryan-Anderson, and B. Neyenhuis, Demonstration of the trapped-ion quantum ccd computer architecture, *Nature* **592**, 209 (2021).
- [8] P. J. J. O'Malley, R. Babbush, I. D. Kivlichan, J. Romero, J. R. McClean, R. Barends, J. Kelly, P. Roushan, A. Tranter, N. Ding, B. Campbell, Y. Chen, Z. Chen, B. Chiaro, A. Dunsworth, A. G. Fowler, E. Jeffrey, E. Lucero, A. Megrant, J. Y. Mutus, M. Neeley, C. Neill, C. Quintana, D. Sank, A. Vainsencher, J. Wenner, T. C. White, P. V. Coveney, P. J. Love, H. Neven, A. Aspuru-Guzik, and J. M. Martinis, Scalable quantum simulation of molecular energies, *Phys. Rev. X* **6**, 031007 (2016).
- [9] A. Kandala, A. Mezzacapo, K. Temme, M. Takita, M. Brink, J. M. Chow, and J. M. Gambetta, Hardware-efficient variational quantum eigensolver for small molecules and quantum magnets, *Nature* **549**, 242 (2017).
- [10] C. Hempel, C. Maier, J. Romero, J. McClean, T. Monz, H. Shen, P. Jurcevic, B. P. Lanyon, P. Love, R. Babbush, A. Aspuru-Guzik, R. Blatt, and C. F. Roos, Quantum chemistry calculations on a trapped-ion quantum simulator, *Phys. Rev. X* **8**, 031022 (2018).
- [11] A. Kandala, K. Temme, A. D. Córcoles, A. Mezzacapo, J. M. Chow, and J. M. Gambetta, Error mitigation extends the computational reach of a noisy quantum processor, *Nature* **567**, 491 (2019).
- [12] F. Arute, K. Arya, R. Babbush, D. Bacon, J. C. Bardin, R. Barends, S. Boixo, M. Broughton, B. B. Buckley, D. A. Buell, B. Burkett, N. Bushnell, Y. Chen, Z. Chen, B. Chiaro, R. Collins, W. Courtney, S. Demura, A. Dunsworth, E. Farhi, A. Fowler, B. Foxen, C. Gidney, M. Giustina, R. Graff, S. Habegger, M. P. Harrigan, A. Ho, S. Hong, T. Huang, W. J. Huggins, L. Ioffe, S. V. Isakov, E. Jeffrey, Z. Jiang, C. Jones, D. Kafri, K. Kechedzhi, J. Kelly, S. Kim, P. V. Klimov, A. Korotkov, F. Kostritsa, D. Landhuis, P. Laptev, M. Lindmark, E. Lucero, O. Martin, J. M. Martinis, J. R. McClean, M. McEwen, A. Megrant, X. Mi, M. Mohseni, W. Mruczkiewicz, J. Mutus, O. Naaman, M. Neeley, C. Neill, H. Neven, M. Y. Niu, T. E. O'Brien, E. Ostby, A. Petukhov, H. Putterman, C. Quintana, P. Roushan, N. C. Rubin, D. Sank, K. J. Satzinger, V. Smelyanskiy, D. Strain, K. J. Sung, M. Szalay, T. Y. Takeshita, A. Vainsencher, T. White, N. Wiebe, Z. J. Yao, P. Yeh, and A. Zalcman, Hartree-fock on a superconducting qubit quantum computer, *Science* **369**, 1084 (2020).
- [13] M. J. Rančić, Exactly solving the Kitaev chain and generating Majorana-zero-modes out of noisy qubits, *Scientific Reports* **12**, 19882 (2022).
- [14] R. M. Lutchyn, E. P. A. M. Bakkers, L. P. Kouwenhoven, P. Krogstrup, C. M. Marcus, and Y. Oreg, Majorana zero modes in superconductor–semiconductor heterostructures, *Nature Reviews Materials* **3**, 52 (2018).
- [15] Z. Jiang, K. J. Sung, K. Kechedzhi, V. N. Smelyanskiy, and S. Boixo, Quantum algorithms to simulate many-body physics of correlated fermions, *Phys. Rev. Applied* **9**, 044036 (2018).
- [16] L. Viola, E. Knill, and S. Lloyd, Dynamical decoupling of open quantum systems, *Phys. Rev. Lett.* **82**, 2417 (1999).
- [17] M. A. Ali Ahmed, G. A. Álvarez, and D. Suter, Robustness of dynamical decoupling sequences, *Phys. Rev. A* **87**, 042309 (2013).
- [18] *Qiskit: An open-source framework for quantum computing* (2022).
- [19] S. Bravyi, S. Sheldon, A. Kandala, D. C. McKay, and J. M. Gambetta, Mitigating measurement errors in multiqubit experiments, *Phys. Rev. A* **103**, 042605 (2021).
- [20] mthree: Matrix-free Measurement Mitigation, <https://github.com/Qiskit-Partners/mthree>, accessed: 2022-03-30.
- [21] P. D. Nation, H. Kang, N. Sundaresan, and J. M. Gambetta, Scalable mitigation of measurement errors on quantum computers, *PRX Quantum* **2**, 040326 (2021).
- [22] R. McWeeny, Some recent advances in density matrix theory, *Rev. Mod. Phys.* **32**, 335 (1960).
- [23] V. Bach, E. H. Lieb, and J. P. Solovej, Generalized Hartree-Fock theory and the Hubbard model, *Journal of Statistical Physics* **76**, 3 (1994).
- [24] mapomatic: Automatic mapping of compiled circuits to low-noise sub-graphs, <https://github.com/Qiskit-Partners/mapomatic>, accessed: 2022-03-30.
- [25] M. Gluza, M. Kliesch, J. Eisert, and L. Aolita, Fidelity witnesses for fermionic quantum simulations, *Phys. Rev. Lett.* **120**, 190501 (2018).
- [26] N. Leumer, M. Marganska, B. Muralidharan, and M. Grifoni, Exact eigenvectors and eigenvalues of the finite Kitaev chain and its topological properties, *Journal of Physics: Condensed Matter* **32**, 445502 (2020).
- [27] N. Harle, O. Shtanko, and R. Movassagh, Observing and braiding topological Majorana modes on programmable quantum simulators (2022), [arXiv:2203.15083](https://arxiv.org/abs/2203.15083) [quant-ph].
- [28] X. Mi, M. Sonner, M. Y. Niu, K. W. Lee, B. Foxen, R. Acharya, I. Aleiner, T. I. Andersen, F. Arute, K. Arya, A. Asfaw, J. Atalaya, J. C. Bardin, J. Basso, A. Bengtsson, G. Bortoli, A. Bourassa, L. Brill, M. Broughton, B. B. Buckley, D. A. Buell, B. Burkett, N. Bushnell, Z. Chen, B. Chiaro, R. Collins, P. Conner, W. Courtney, A. L. Crook, D. M. Debroy, S. Demura, A. Dunsworth, D. Eppens, C. Erickson, L. Faoro, E. Farhi, R. Fatemi, L. Flores, E. Forati, A. G. Fowler, W. Giang, C. Gidney, D. Gilboa, M. Giustina, A. G. Dau, J. A. Gross, S. Habegger, M. P. Harrigan, M. Hoffmann, S. Hong, T. Huang, A. Huff, W. J. Huggins, L. B. Ioffe, S. V. Isakov, J. Iveland, E. Jeffrey, Z. Jiang, C. Jones, D. Kafri, K. Kechedzhi, T. Khattar, S. Kim, A. Y. Kitaev, P. V. Klimov, A. R. Klots, A. N. Korotkov, F. Kostritsa, J. M. Kreikebaum, D. Landhuis, P. Laptev, K.-M. Lau, J. Lee, L. Laws, W. Liu, A. Locharla, O. Martin, J. R. McClean, M. McEwen, B. M. Costa, K. C. Miao, M. Mohseni, S. Montazeri, A. Morvan, E. Mount, W. Mruczkiewicz, O. Naaman, M. Neeley, C. Neill, M. Newman, T. E. O'Brien, A. Opremcak, A. Petukhov, R. Potter, C. Quintana, N. C. Rubin, N. Saei, D. Sank, K. Sankaragomathi, K. J. Satzinger, C. Schuster, M. J. Shearn, V. Shvarts, D. Strain, Y. Su, M. Szalay, G. Vidal, B. Villalonga, C. Vollgraf-Heidweiller, T. White, Z. Yao, P. Yeh, J. Yoo, A. Zalcman, Y. Zhang, N. Zhu, H. Neven, D. Bacon, J. Hilton, E. Lucero, R. Babbush, S. Boixo, A. Megrant, Y. Chen, J. Kelly, V. Smelyanskiy, D. A.

- Abanin, and P. Roushan, Noise-resilient edge modes on a chain of superconducting qubits, *Science* **378**, 785 (2022), <https://www.science.org/doi/pdf/10.1126/science.abq5769>.
- [29] L. Fidkowski and A. Kitaev, Effects of interactions on the topological classification of free fermion systems, *Phys. Rev. B* **81**, 134509 (2010).
- [30] L. Fidkowski and A. Kitaev, Topological phases of fermions in one dimension, *Phys. Rev. B* **83**, 075103 (2011).
- [31] S. Gangadharaiah, B. Braunecker, P. Simon, and D. Loss, Majorana edge states in interacting one-dimensional systems, *Phys. Rev. Lett.* **107**, 036801 (2011).
- [32] A. Rahmani, X. Zhu, M. Franz, and I. Affleck, Emergent supersymmetry from strongly interacting Majorana zero modes, *Phys. Rev. Lett.* **115**, 166401 (2015).
- [33] J.-J. Miao, H.-K. Jin, F.-C. Zhang, and Y. Zhou, Exact solution for the interacting Kitaev chain at the symmetric point, *Phys. Rev. Lett.* **118**, 267701 (2017).
- [34] J. P. T. Stenger, G. Ben-Shach, D. Pekker, and N. T. Bronn, Simulating spectroscopy experiments with a superconducting quantum computer, *Physical Review Research* **4**, 043106 (2022).
- [35] A. Peruzzo, J. McClean, P. Shadbolt, M.-H. Yung, X.-Q. Zhou, P. J. Love, A. Aspuru-Guzik, and J. L. O'Brien, A variational eigenvalue solver on a photonic quantum processor, *Nature Communications* **5**, 1 (2014).
- [36] M. Cerezo, A. Arrasmith, R. Babbush, S. C. Benjamin, S. Endo, K. Fujii, J. R. McClean, K. Mitarai, X. Yuan, L. Cincio, and P. J. Coles, Variational quantum algorithms, *Nature Reviews Physics* **3**, 625 (2021).
- [37] E. Farhi, J. Goldstone, S. Gutmann, and M. Sipser, *Quantum computation by adiabatic evolution* (2000).
- [38] D. Aharonov, W. van Dam, J. Kempe, Z. Landau, S. Lloyd, and O. Regev, Adiabatic quantum computation is equivalent to standard quantum computation, *SIAM Journal on Computing* **37**, 166 (2007), <https://doi.org/10.1137/S0097539705447323>.
- [39] qpic: Creating quantum circuit diagrams in TikZ, <https://github.com/qpic/qpic>, accessed: 2022-04-07.
- [40] J. D. Hunter, Matplotlib: A 2d graphics environment, *Computing in Science & Engineering* **9**, 90 (2007).
- [41] J. R. McClean, N. C. Rubin, K. J. Sung, I. D. Kivlichan, X. Bonet-Monroig, Y. Cao, C. Dai, E. S. Fried, C. Gidney, B. Gimby, P. Gokhale, T. Häner, T. Hardikar, V. Havlíček, O. Higgott, C. Huang, J. Izaac, Z. Jiang, X. Liu, S. McArdle, M. Neeley, T. O'Brien, B. O'Gorman, I. Ozfidan, M. D. Radin, J. Romero, N. P. D. Sawaya, B. Senjean, K. Setia, S. Sim, D. S. Steiger, M. Steudtner, Q. Sun, W. Sun, D. Wang, F. Zhang, and R. Babbush, OpenFermion: the electronic structure package for quantum computers, *Quantum Science and Technology* **5**, 034014 (2020).

Author contributions

N.T.B. and O.T.L. conceived the project. K.J.S. developed the error mitigation techniques and collected and analyzed the experimental data. K.J.S. and N.T.B. wrote the software for the experiment. K.J.S. and M.J.R. wrote the manuscript with the assistance of N.T.B. and O.T.L. All authors contributed to discussions that shaped the

project.

Competing interests

The authors declare no competing interests.

Appendix A: Fermionic Gaussian states

In this section, we provide background material on fermionic Gaussian states and review the quantum algorithm given in Reference [15] for preparing them.

Fermionic Gaussian states can be defined in several equivalent ways. One definition is that fermionic Gaussian states are eigenstates of quadratic fermionic Hamiltonians. The general form of a quadratic fermionic Hamiltonian can be written as

$$H = \sum_{p,q=1}^n M_{pq} a_p^\dagger a_q + \frac{1}{2} \sum_{p,q=1}^n (\Delta_{pq} a_p^\dagger a_q^\dagger - \Delta_{pq}^* a_p a_q), \quad (\text{A1})$$

where M and Δ are $n \times n$ matrices. The operators $\{a_p\}_{p=1}^n$ are fermionic annihilation operators which satisfy the fermionic anticommutation relations

$$a_p a_q + a_q a_p = 0, \quad (\text{A2})$$

$$a_p a_q^\dagger + a_q^\dagger a_p = \delta_{pq}. \quad (\text{A3})$$

The adjoint a_p^\dagger of an annihilation operator a_p is called a creation operator. Since H is Hermitian, we must have $M = M^\dagger$ and $\Delta = -\Delta^T$. Any quadratic Hamiltonian can be rewritten in the following form:

$$H = \sum_{p=1}^n \varepsilon_p b_p^\dagger b_p + \text{constant}, \quad (\text{A4})$$

where the ε_p are non-negative real numbers. The $\{b_p\}$ are a new set of fermionic annihilation operators that also satisfy the anticommutation relations (A2) and (A3). They are linear combinations of the original creation and annihilation operators:

$$\begin{pmatrix} b_1^\dagger \\ \vdots \\ b_n^\dagger \\ b_1 \\ \vdots \\ b_n \end{pmatrix} = W \begin{pmatrix} a_1^\dagger \\ \vdots \\ a_n^\dagger \\ a_1 \\ \vdots \\ a_n \end{pmatrix}, \quad (\text{A5})$$

where W is a $2n \times 2n$ matrix. The matrix W is unitary and has the block form

$$W = \begin{pmatrix} W_1^* & W_2^* \\ W_2 & W_1 \end{pmatrix}, \quad (\text{A6})$$

where the fermionic anticommutation relations imply that

$$W_1 W_2^T + W_2 W_1^T = 0, \quad (\text{A7})$$

$$W_1 W_1^\dagger + W_2 W_2^\dagger = I. \quad (\text{A8})$$

The matrix W can be efficiently computed from M and Δ using a Schur decomposition; we refer the reader to Appendix A of Reference [15] for a detailed description of how to perform this computation. Source code for performing this computation is available in both OpenFermion [41] and Qiskit Nature [18].

A fermionic Gaussian state can be prepared as an eigenstate of the Hamiltonian (A1) by effecting a unitary transformation \mathcal{W} such that

$$\mathcal{W} a_p \mathcal{W}^\dagger = b_p, \quad p = 1, \dots, n. \quad (\text{A9})$$

Up to a global phase, this unitary is determined by the matrix W . The ground state of H is

$$|\Psi_0\rangle = \mathcal{W}|\text{vac}\rangle, \quad (\text{A10})$$

and the other eigenstates are of the form

$$\left(b_1^\dagger\right)^{i_1} \cdots \left(b_n^\dagger\right)^{i_n} |\Psi_0\rangle, \quad (\text{A11})$$

where $i_p \in \{0, 1\}$ for $p = 1, \dots, n$. Therefore, a fermionic Gaussian state is prepared by applying \mathcal{W} to a state of the form

$$\left(a_1^\dagger\right)^{i_1} \cdots \left(a_n^\dagger\right)^{i_n} |\text{vac}\rangle, \quad (\text{A12})$$

a computational basis state under the Jordan-Wigner transformation.

To implement the unitary, we used the algorithm described in Reference [15]. The algorithm starts with the matrix W as input. Actually, due to the redundancy in W only the lower half W_L is used:

$$W_L = (W_2 \quad W_1). \quad (\text{A13})$$

The algorithm works by finding a decomposition of W_L

$$V W_L U^\dagger = (0 \quad I), \quad (\text{A14})$$

where I is the identity matrix, V is an $n \times n$ unitary matrix, and U is further decomposed into elementary matrix operations as

$$U = B G_{n_G} \cdots B G_3 G_2 B G_1 B. \quad (\text{A15})$$

Here, each G_i is a matrix of the form

$$G(\theta, \varphi) = \left(\begin{array}{cc|cc} \cos \theta & -e^{i\varphi} \sin \theta & 0 & 0 \\ \sin \theta & e^{i\varphi} \cos \theta & 0 & 0 \\ \hline 0 & 0 & \cos \theta & -e^{-i\varphi} \sin \theta \\ 0 & 0 & \sin \theta & e^{-i\varphi} \cos \theta \end{array} \right), \quad (\text{A16})$$

and

$$B = B^\dagger = \begin{pmatrix} I - e_n e_n^T & e_n e_n^T \\ e_n e_n^T & I - e_n e_n^T \end{pmatrix}, \quad (\text{A17})$$

where $e_n = (0, \dots, 0, 1)^T$ is a vector of length n . The decomposition (A14) corresponds to a decomposition

$$\mathcal{W} = \mathcal{B} \mathcal{G}_1 \mathcal{B} \mathcal{G}_2 \mathcal{G}_3 \mathcal{B} \cdots \mathcal{G}_{n_G} \mathcal{B} \cdot \mathcal{V} = \mathcal{U} \cdot \mathcal{V} \quad (\text{A18})$$

of the desired unitary in terms of elementary gates. Here each \mathcal{G}_i is a complex Givens rotation gate of the form

$$\mathcal{G}(\theta, \varphi) = \exp[i\varphi a_q^\dagger a_q] \exp[\theta(a_p^\dagger a_q - a_q^\dagger a_p)] \quad (\text{A19})$$

acting on neighboring modes, and \mathcal{B} is the particle-hole transformation on the last fermionic mode,

$$\mathcal{B} a_n \mathcal{B}^\dagger = a_n^\dagger, \quad (\text{A20})$$

$$\mathcal{B} a_p \mathcal{B}^\dagger = a_p \quad \text{for } p = 1, \dots, n-1. \quad (\text{A21})$$

Under the Jordan-Wigner transformation, the Givens rotation between neighboring modes is a two-qubit gate with matrix

$$G(\theta, \varphi) = \begin{pmatrix} 1 & 0 & 0 & 0 \\ 0 & e^{i\varphi} \cos(\theta) & -e^{i\varphi} \sin(\theta) & 0 \\ 0 & \sin(\theta) & \cos(\theta) & 0 \\ 0 & 0 & 0 & e^{i\varphi} \end{pmatrix}, \quad (\text{A22})$$

and the particle-hole transformation is a single-qubit X gate on the last qubit. The unitary \mathcal{V} can also be decomposed into Givens rotations, but this is not necessary when the initial state of the circuit is the all zeros state, i.e., when the ground state is being prepared. The total number of Givens rotations used by the algorithm is

$$\frac{n(n-1)}{2} + \eta(n-\eta) \quad (\text{A23})$$

where η is the number of pseudoparticles. The circuit depth is at most $3n-2$.

In summary, this algorithm yields a quantum circuit for preparing the fermionic Gaussian state under the Jordan-Wigner transformation with linear depth and which uses only linear connectivity. Source code for this algorithm is available in both OpenFermion [41] and Qiskit Nature [18].

Appendix B: Measurement of the correlation matrix

In this section, we provide details on our strategy for measuring the correlation matrix of a fermionic Gaussian state. Our strategy is similar to the one used in Reference [12] to measure the one-particle reduced density matrix (1-RDM).

The correlation matrix Γ of a state ρ is defined as the block matrix

$$\Gamma = \begin{pmatrix} T & S \\ -S^* & I - T^T \end{pmatrix} \quad (\text{B1})$$

where

$$T_{jk} = \text{Tr} \left[a_j^\dagger a_k \rho \right] \quad (\text{B2})$$

$$S_{jk} = \text{Tr} \left[a_j^\dagger a_k^\dagger \rho \right] \quad (\text{B3})$$

and I is the identity matrix.

The diagonal entries of the correlation matrix are occupation numbers that can be measured straightforwardly in the computational basis. To obtain the off-diagonal entries, we need to measure the operators

$$a_j^\dagger a_k + a_k^\dagger a_j \mapsto \frac{X_j X_k + Y_j Y_k}{2} Z_{j+1} \cdots Z_{k-1} \quad (\text{B4})$$

$$-i(a_j^\dagger a_k - a_k^\dagger a_j) \mapsto \frac{X_j Y_k - Y_j X_k}{2} Z_{j+1} \cdots Z_{k-1} \quad (\text{B5})$$

$$a_j^\dagger a_k^\dagger + a_k a_j \mapsto \frac{X_j X_k - Y_j Y_k}{2} Z_{j+1} \cdots Z_{k-1} \quad (\text{B6})$$

$$-i(a_j^\dagger a_k^\dagger - a_k a_j) \mapsto \frac{-X_j Y_k - Y_j X_k}{2} Z_{j+1} \cdots Z_{k-1} \quad (\text{B7})$$

where $j < k$ and we have shown how the operators map under the Jordan-Wigner transformation. For the case of neighboring modes, i.e., $k = j + 1$, we have

$$a_j^\dagger a_k + a_k^\dagger a_j \mapsto \frac{X_j X_k + Y_j Y_k}{2} \quad (\text{B8})$$

$$-i(a_j^\dagger a_k - a_k^\dagger a_j) \mapsto \frac{X_j Y_k - Y_j X_k}{2} \quad (\text{B9})$$

$$a_j^\dagger a_k^\dagger + a_k a_j \mapsto \frac{X_j X_k - Y_j Y_k}{2} \quad (\text{B10})$$

$$-i(a_j^\dagger a_k^\dagger - a_k a_j) \mapsto \frac{-X_j Y_k - Y_j X_k}{2}. \quad (\text{B11})$$

If the correlation matrix is real, then only the first and third operators need to be measured. A sufficient condition for the correlation matrix to be real is that the circuit used to prepare the state contains only gates with real-valued matrices, up to global phase. In our experiment, we checked for this condition by directly inspecting the gates in the circuit.

Between neighboring modes, these operators can be measured by diagonalizing them with a parity-preserving two-qubit gate. For example, the third operator is diagonalized by the gate with matrix

$$\begin{pmatrix} \frac{1}{\sqrt{2}} & 0 & 0 & \frac{1}{\sqrt{2}} \\ 0 & 1 & 0 & 0 \\ 0 & 0 & 1 & 0 \\ -\frac{1}{\sqrt{2}} & 0 & 0 & \frac{1}{\sqrt{2}} \end{pmatrix}. \quad (\text{B12})$$

Using parity-preserving gates for measurement enables the error mitigation technique of postselection on bitstring parity, described below. These gates can be implemented on hardware similarly to the Givens rotation

gates by decomposing them into two CNOT gates plus single-qubit rotations.

To measure the operators between non-neighboring modes, there are several possible approaches. One could measure them directly in the Pauli basis using single-qubit rotations to effect the basis changes. This approach has the drawback that the single-qubit rotations do not preserve the parity, so we would not be able to perform bitstring postselection on parity. Alternatively, one could perform fermionic swap gates to swap the modes until they are neighboring. However, this approach involves adding additional gates to the circuits, which increases the errors due to execution on a noisy device.

Here, we take a different approach, which was described in Reference [12] for the case of measuring the 1-RDM of a Slater determinant. Recall that the fermionic Gaussian state is prepared by effecting a unitary transformation \mathcal{W} such that

$$\mathcal{W} a_p \mathcal{W}^\dagger = b_p, \quad p = 1, \dots, n. \quad (\text{B13})$$

The $\{b_j^\dagger\}$ are linear combinations of the original creation and annihilation operators:

$$\begin{pmatrix} b_1^\dagger \\ \vdots \\ b_n^\dagger \end{pmatrix} = W \begin{pmatrix} a_1^\dagger \\ \vdots \\ a_n^\dagger \\ a_1 \\ \vdots \\ a_n \end{pmatrix} \quad (\text{B14})$$

where W is an $n \times 2n$ matrix. The matrix W can be efficiently computed from the description of the Hamiltonian and is used to produce the quantum circuit that prepares an eigenstate of the Hamiltonian, as described in Appendix A. Note that the columns of W are indexed by the operators $\{a_j^\dagger\}$ and $\{a_j\}$. However, the ordering of the operators $\{a_j^\dagger\}$ is arbitrary, so we can reorder them without changing the definition of the $\{b_j^\dagger\}$ and the target fermionic Gaussian state. A reordering of the operators $\{a_j^\dagger\}$ corresponds to a permutation of the first n columns of W . We want to use the same order for both the $\{a_j^\dagger\}$ and the $\{a_j\}$, so we will always apply the same permutation to the first n columns of W and the last n columns. Each permutation causes different pairs of modes to be mapped to neighboring qubits. This procedure enables the measurement of operators between all pairs of modes without the need to add fermionic swap gates to the circuits. By generating the permutations according to a ‘‘parallel bubble sort’’ pattern, we can minimize the total number of permutations needed.

As an example, consider a system of 6 fermionic modes, initially labeled as

$$(0, 1, 2, 3, 4, 5) \quad (\text{B15})$$

In this configuration, we can measure the operators between 0–1, 1–2, etc. The parallel bubble sort pattern performs a sequence of swaps starting on even indices, followed by a sequence of swaps on odd indices:

$$(0, 1, 2, 3, 4, 5) \rightarrow (1, 0, 3, 2, 5, 4) \rightarrow (1, 3, 0, 5, 2, 4). \quad (\text{B16})$$

Now, we can measure the operators between 1–3, 0–5, etc. Repeating this procedure one more time yields the configuration (3, 5, 1, 4, 0, 2), allowing the rest of the operators to be measured. In total, $\lceil n/2 \rceil$ permutations are required, including the identity permutation corresponding to the initial configuration. For each permutation, four different basis changes are required to measure the operators (B8–B11), and each basis change gives rise to two circuits, one to measure pairs of qubits starting on even indices, and one for odd indices. Together with the circuit for measuring the diagonal entries, measuring the correlation matrix of a state requires $\lceil n/2 \rceil \times 8 + 1$ circuits in total. In our experiments the correlation matrix was real, so only two of the basis changes were required and the total number of circuits was $\lceil n/2 \rceil \times 4 + 1$.

Appendix C: Fidelity witness

Reference [25] shows how to obtain a fidelity witness for experiments preparing fermionic Gaussian states. In this section we review this result and describe how we computed the fidelity witness in our experiment.

Consider an experiment that aims to prepare a known pure fermionic Gaussian target state ρ_t . Let ρ_p denote the imperfect state that is actually prepared in the experiment. The closeness between the two states is measured by the fidelity

$$F(\rho_t, \rho_p) = \left(\text{Tr} \left[(\sqrt{\rho_t} \rho_p \sqrt{\rho_t})^{\frac{1}{2}} \right] \right)^2. \quad (\text{C1})$$

Since ρ_t is pure, this equation simplifies to

$$F(\rho_t, \rho_p) = \text{Tr}[\rho_t \rho_p]. \quad (\text{C2})$$

A fidelity witness is an observable W for which the value $F_W(\rho_p) = \text{Tr}[W \rho_p]$ gives a lower bound on the fidelity between ρ_t and ρ_p . Reference [25] describes such a witness and gives an expression for the fidelity lower bound in terms of the covariance matrices M_t and M_p of ρ_t and ρ_p :

$$F_W(\rho_p) = 1 + \frac{1}{4} \text{Tr}[(M_p - M_t)^T M_t] \quad (\text{C3})$$

The covariance matrix M of a state ρ has entries

$$M_{jk} = \frac{i}{2} \text{Tr}[(\gamma_j \gamma_k - \gamma_k \gamma_j) \rho] \quad (\text{C4})$$

where the γ_j are Majorana fermion operators. To relate the covariance matrix to the correlation matrix it is

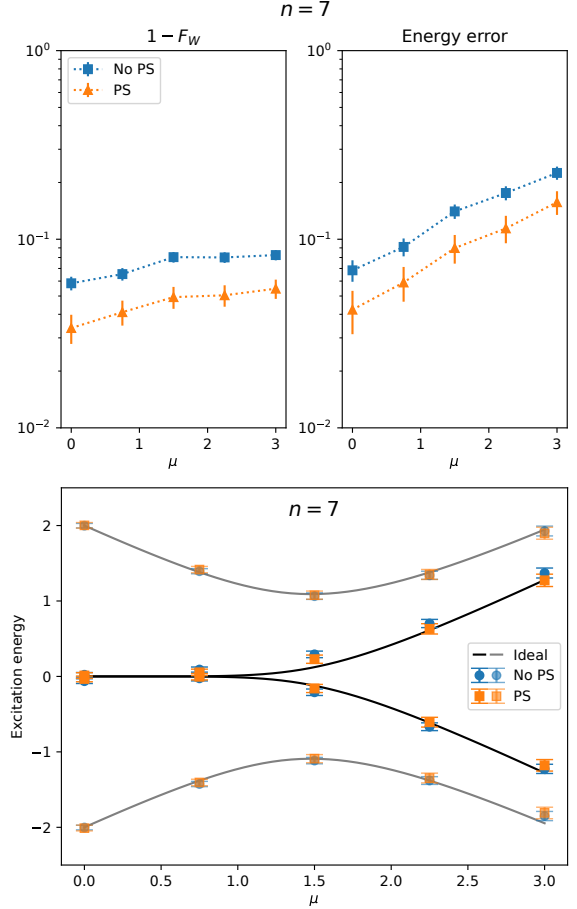


FIG. 6. Effectiveness of post-selection. Data is presented for the Kitaev chain of length 7. (Top) Fidelity witness and energy error for the data analyzed without postselection (No PS) and with postselection (PS). (Bottom) Measured excitation energies with and without postselection.

convenient to use the following alternative indexing convention for the Majorana operators:

$$\gamma_j = a_j + a_j^\dagger, \quad \gamma_{j+n} = -i(a_j - a_j^\dagger). \quad (\text{C5})$$

Under this convention, the covariance matrix is related to the correlation matrix Γ by the identity

$$M = i\Omega(2\Gamma - I)\Omega^\dagger \quad (\text{C6})$$

where Ω is the block matrix

$$\Omega = \frac{1}{\sqrt{2}} \begin{pmatrix} I & I \\ iI & -iI \end{pmatrix}. \quad (\text{C7})$$

Using this relation, the expression for the fidelity lower bound can be written in terms of the correlation matrices Γ_t and Γ_p of ρ_t and ρ_p :

$$F_W(\rho_p) = 1 - \text{Tr} \left[(\Gamma_t - \Gamma_p) \left(\Gamma_t - \frac{I}{2} \right) \right]. \quad (\text{C8})$$

While Reference [25] describes an efficient protocol for measuring the fidelity lower bound without needing to measure the entire covariance or correlation matrix, in our experiment we measured the entire correlation matrix and directly used Equation (C8) to compute the fidelity lower bound.

Appendix D: Effect of postselection

In this section, we provide additional data demonstrating the effect of the error mitigation technique of postselection on bitstring parity. Figure 6 shows the fidelity witness, energy error, and excitation energies for the data from the 7-qubit experiment, analyzed with and without postselection. All the other error mitigation techniques are still applied. The data shows that while postselection does give a noticeable improvement to fidelity and energy precision, the energy curves are still reproduced quite well without it, including the measurement of the zero-energy excitation states.